Influence of bimodal copper grain size distribution on electrical resistivity and tensile strength of silver - copper composite wires

Simon Tardieu, David Mesguich, Antoine Lonjon, Florence Lecouturier-Dupouy, Nelson Ferreira, Geoffroy Chevallier, Arnaud Proietti, Claude Estournès, Christophe Laurent

Influence of bimodal copper grain size distribution on electrical resistivity and tensile strength of silver - copper composite wires

Simon Tardieu, David Mesguich, Antoine Lonjon, Florence Lecouturier-Dupouy, Nelson Ferreira, Geoffroy Chevallier, Arnaud Proietti, Claude Estournès, Christophe Laurent

PII: S2352-4928(23)02094-9

DOI: https://doi.org/10.1016/j.mtcomm.2023.107403

Reference: MTCOMM107403

To appear in: *Materials Today Communications*

Received date: 26 July 2023
Revised date: 19 October 2023
Accepted date: 21 October 2023

Please cite this article as: Simon Tardieu, David Mesguich, Antoine Lonjon, Florence Lecouturier-Dupouy, Nelson Ferreira, Geoffroy Chevallier, Arnaud Proietti, Claude Estournès and Christophe Laurent, Influence of bimodal copper grain size distribution on electrical resistivity and tensile strength of silver - copper composite wires, *Materials Today Communications,* (2023) doi:https://doi.org/10.1016/j.mtcomm.2023.107403

Influence of bimodal copper grain size distribution on electrical resistivity and tensile strength of silver - copper composite wires

Simon Tardieu[a], David Mesguich[b], Antoine Lonjon[b], Florence Lecouturier-Dupouy[a], Nelson Ferreira[a], Geoffroy Chevallier[b,c], Arnaud Proietti[d], Claude Estournès[b,c], Christophe Laurent[b]

[a] CNRS, Laboratoire National des Champs Magnétiques Intenses, INSA-UGA-UPS-EMFL, Grenoble & Toulouse, France.

[b] CIRIMAT, Université Toulouse 3 Paul Sabatier, Toulouse INP, CNRS, Université de Toulouse, 118 route de Narbonne, F-31062 Toulouse cedex 9, France.

[c] Plateforme Nationale CNRS de Frittage Flash, Université Toulouse 3 Paul Sabatier, PNF², MHT, 118 route de Narbonne, F-31062 Toulouse cedex 9, France.

[d] Université de Toulouse, Centre de Microcaractérisation Raimond Castaing, UAR 3623, Espace Clément Ader, 3 rue Caroline Aigle, 31400 Toulouse, France

e-mail addresses of all authors:

simon.tardieu@lncmi.cnrs.fr

david.mesguich@univ-tlse3.fr

antoine.lonjon@univ-tlse3.fr

florence.lecouturier@lncmi.cnrs.fr

nelson.ferreira@lncmi.cnrs.fr

geoffroy.chevallier@univ-tlse3.fr

arnaud.proietti@ums-castaing.fr

claude.estournes@univ-tlse3.fr

christophe.laurent@univ-tlse3.fr

ABSTRACT

In order to obtain the best compromise between high strength and low resistivity it was decided to introduce a controlled content of copper (Cu) large grains in copper-silver (Ag-Cu) composite wires. Composite powders are prepared by mixing of 1 vol. % Ag nanowires and bimodal Cu powder. The so-obtained composites powders are consolidated into cylinders (8 mm in diameter and 30 mm long) by

Spark Plasma Sintering (SPS) at only 450 °C. The cylinders served as starting materials for room temperature wire-drawing (WD) for the preparation of fine wires (1-0.2 mm diameter). The microstructure of the cylinders and the wires was investigated by scanning electron microscopy imaging and electron backscattered diffraction analysis. The electrical resistivity and the tensile strength were measured at 293 K and 77 K. The electrical resistivity of the wires is the lowest when the large Cu grain content is the highest. Cu large grains greatly limit the electronic scattering, forming areas with few grain boundaries and no Ag/Cu interfaces and therefore can be considered as fast conduction channels. Conversely, the addition of Cu large grains leads to a moderate decrease in mechanical strength. By presenting a 12 % lower electrical resistivity and an equivalent ultimate tensile strength (UTS) wires with bimodal Cu matrix show a better compromise between low electrical resistivity and high UTS (0.45 μΩ.cm, 1082 MPa at 77 K) compared to wires with a fine-grained Cu matrix (0.51 μΩ.cm, 1138 MPa at 77 K).

KEYWORDS

Coil Materials; Composites; Copper; Silver Nanowires; Spark Plasma Sintering; Wire-Drawing

1 INTRODUCTION

A very high energy of the order of several megajoules must be injected into an appropriate coil in order to generate non-destructive pulsed magnetic fields. The wires that make up the coil must have an electrical resistivity as close as possible to that of pure annealed Cu in order to maximize the duration of the pulse. Although they are immersed in liquid nitrogen in order to limit the heating due to the Joule effect, the pulse is limited to a short duration (i.e. few ms). Moreover, the conductors must show a very high mechanical strength in order to withstand the stresses caused by the Lorentz forces induced by the generation of the magnetic field (1 GPa at 60 T and higher than 2.2 GPa at 100 T [1]). Solutions have been proposed to prepare high-strength low-resistivity wires and they involve Cu-based alloys and/or Cu-based composites. Ag/Cu (6-24 wt. % Ag) alloy wires are prepared by metallurgy routes involving high temperatures (melting, solidification and drawing) [2-5]. They exhibit a high ultimate tensile strength (UTS) of 1160 MPa at 77 K, but the eutectic microstructure (a mixture of Cu-rich and Ag-rich

solid solutions) and a high Ag total content are responsible for a high electrical resistivity (2.10 to 2.65 μΩ.cm at room temperature and about 0.80 μΩ.cm at 77 K). Thus, Ag/Cu alloy conductors are unsuitable for the winding of coils for non-destructive pulsed magnetic fields. Composite wires, i.e. pure Cu matrix reinforced by a second phase, have also been investigated [6-15]. The need to avoid alloying during both the design and process of the Ag-Cu composite wires has also been evidenced [15]. Moreover, it has been shown that Ag-Cu composite wires containing only 1 vol. % Ag offer the best combination of high UTS (1000 MPa at 77 K) and low electrical resistivity (0.44 μΩ cm at 77 K) over samples with 5 vol. % Ag (1300 MPa and 0.7 μΩ.cm at 77 K) [14]. Several studies [13-18] have indicated that a promising route to increase strength and ductility without increasing resistivity is to use a metallic sample with a bimodal grain size, because of a combination of Orowan strengthening, strain hardening and the presence of large channels for fast electron transport. Therefore, the aim of this work is to prepare and study 1 vol. % Ag-Cu composite wires with a Cu matrix showing a bimodal grain-size distribution. A schematic representation of the method and the expected microstructures of the samples is presented in Fig. 1.

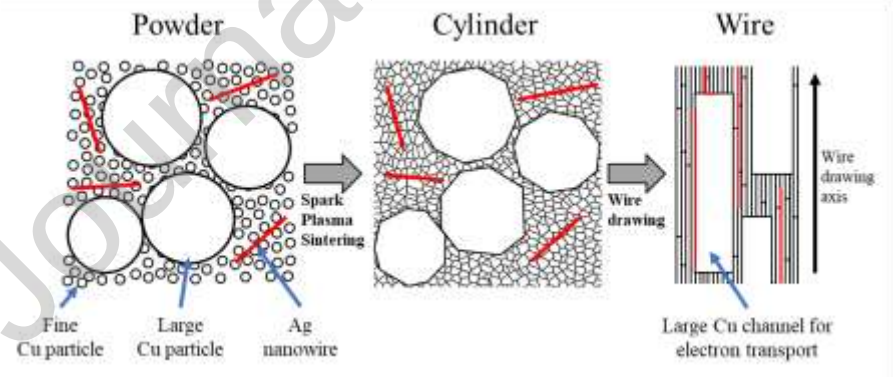

Fig. 1. Schematic representation of the method and the expected microstructure of the powder, cylinder and wire samples.

2 EXPERIMENTAL PROCEDURE

2.1 Powder preparation

The fine Cu powder (Alfa Aesar, purity > 99 %) shows spherical micrometric particles about 1 µm in diameter (d_{10} = 0.58 µm, d_{50} = 1.03 µm, d_{90} = 3.14 µm). This powder will be noted $Cu_{1µm}$ hereafter. The coarse Cu powder (purity > 99.95 %) was prepared by atomization [19] and shows spherical particles about 20 µm in diameter (d_{10} = 5.4 µm, d_{50} = 19.4 µm, d_{90} = 42.5 µm). This powder will be noted $Cu_{20µm}$ hereafter. The two Cu powders are mixed to obtain a homogeneous Cu powder with a bimodal particle size distribution. Two batches of 15 g were prepared, 50/50 and 75/25 in weight ($Cu_{1µm}$/$Cu_{20µm}$). Mixing is carried out with a three-dimensional tumbling mixer (Turbula) (2 h, 3 alumina cylinders, diameter 9 mm, length 10 mm, powder/cylinders weight ratio = 1). Ag-Cu composite powders (1 vol. % Ag) were prepared according to a protocol presented elsewhere [14]. The appropriate amount of bimodal Cu powder was added to a suspension of Ag nanowires (diameter 0.2 µm, length 30 µm, prepared in house [20]) in ethanol and stirred using an ultrasonic probe. Ethanol was removed using a rotary evaporator (80 °C). The 1 vol. % Ag-Cu composite powders are designated $P_{50/50}$ and $P_{75/25}$ hereafter. In order to reduce any Cu oxide at the surface of the Cu particles, the powders were heated to 230 °C (2.5 °C.min^{-1}, 1 h) in a flow of H_2 (15 L/h).

2.2 Spark Plasma Sintering and wire-drawing

The Ag-Cu composite powders were sintered into cylinders by Spark Plasma Sintering (SPS) (PNF^2 Toulouse, Dr. Sinter 2080, SPS Syntex Inc., Japan) according to a procedure described elsewhere [14] [15]. The sample is heated at 25 °C.min^{-1} from room temperature to 450 °C and a 5 min dwell is applied. A uniaxial pressure (30 MPa) is applied gradually during the first minute of the dwell and is maintained for 4 min. As highlighted in a previous study, the sintering temperature should not be too high in order to avoid the formation of Ag/Cu alloys [15]. At 450 °C, the solubility of Ag in Cu is about 0.3 vol. % Ag. For a 5 min dwell at 450 °C, the calculated length of diffusion of Ag in Cu is 16 nm. These values are in line with the hypotheses that 450 °C is a sintering temperature low enough to avoid the formation of Ag/Cu alloys. The so-obtained cylinders (diameter 8 mm and length 30 mm) are designated respectively $C_{50/50}$ and $C_{75/25}$ hereafter. The cylinders were deformed by wire-drawing (WD)

at room temperature through conical WC dies, in about 49 steps, to prepare wires with decreasing diameters down to 0.2 mm. Wire samples were typically 350 mm long. The wires are designated hereafter according to the starting cylinder: for example, wire $W_{75/25}$ is a wire drawn from cylinder $C_{75/25}$. The characterization of the microstructure of the wires was performed on sample with a diameter of 0.5 mm.

2.3 Characterization

The powders were observed by field-emission gun scanning electron microscopy (FEG-SEM, JEOL JSM 6700F). After a preparation by ion milling, using a cross section polisher (JEOL IB-19510CP), the microstructure of the cylinders and wires was investigated by electron backscattered diffraction (EBSD) (NordlysNano, Oxford Instruments) combined with an energy dispersive X-ray spectrometer (EDS) (X-max 80mm², Oxford Instruments) on a FEG-SEM JEOL JSM 7100F TTLS LV. The density of the cylinders was measured by Archimedes' method. Tensile tests (INSTRON 1195 machine) were performed at 293 K and 77 K on 170 mm long wires. Precise stresses were measured by the stress gauge system (1000 N or 250 N, 1.6×10^{-5} m.s^{-1}). The electrical resistivity of 350 mm long wires was measured at 293 K and 77 K using the four-probe method with a maximum current of 100 mA to avoid heating the wires.

3 RESULTS AND DISCUSSION

SEM images of powders $P_{50/50}$ (Fig. 2a) and $P_{75/25}$ (Fig. 2d) clearly reveal the Cu particles originating from the $Cu_{1\mu m}$ and $Cu_{20\mu m}$ powders. The Ag nanowires are mainly evenly distributed with the finer Cu particles but some are located on the surface of the large Cu particles. Higher magnification SEM images of the powders before (Fig. 2b, 2e) and after (Fig. 2c, 2f) the H_2 reduction show that the Cu particles in the reduced samples have a smooth surface, which reflects the elimination of surface oxides.

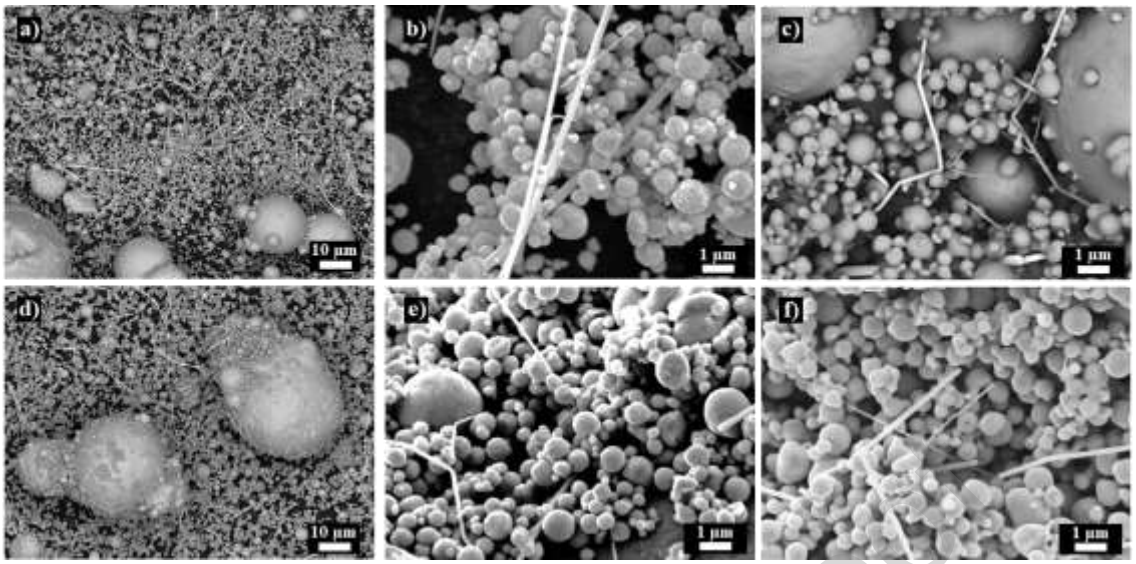

Fig. 2. SEM image of $P_{50/50}$ before reduction (a); higher magnification images of $P_{50/50}$ before (b) and after (c) reduction; SEM image of $P_{75/25}$ before reduction (d); higher magnification images of $P_{75/25}$ before (e) and after (f) reduction.

The relative density of cylinders $C_{50/50}$ and $C_{75/25}$ is 96.7 ± 1.0 % and 95.5 ± 1.0 %, respectively. Non-negligible residual porosity does facilitate the deformation, higher densifications hamper wire-drawing. SEM images of transverse sections of the $C_{50/50}$ and $C_{75/25}$ (Fig. 3) cylinders clearly reveal the residual porosity (appearing black on the images) and the bimodal size of the Cu grains. The larger ones, originating from the $Cu_{20\mu m}$ powder present ∑3 twin boundaries. The smaller Cu grains, originating from the $Cu_{1\mu m}$ powder, are more difficult to distinguish. Nanoscale Ag (appearing white on the images) is observed, reflecting a good dispersion in the fine-grains areas, although some micrometer-sized agglomerates are detected. Very large Ag agglomerates several tens of micrometers long are occasionally observed at the interfaces between large grain and fine grain (indicated by an arrow in Fig. 3).

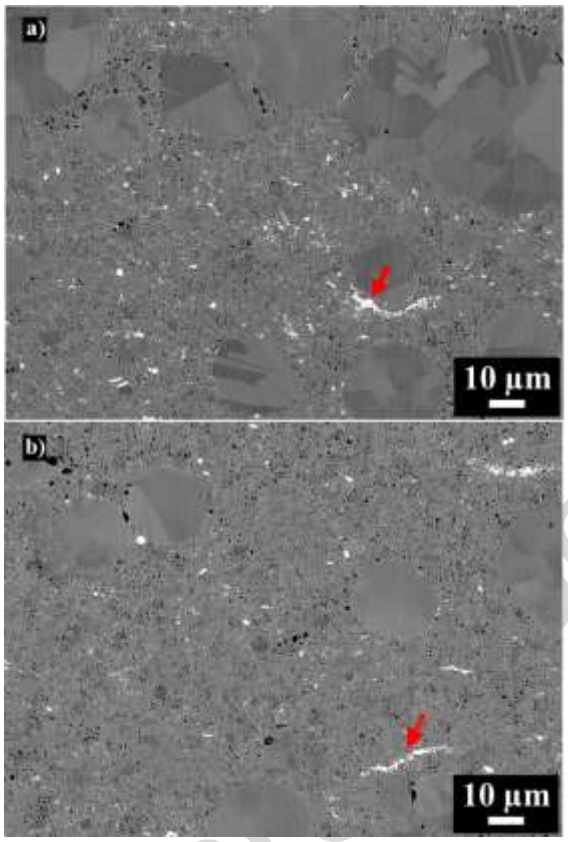

Fig. 3. Backscattered electrons SEM images (BSE) of transverse sections of the (a) $C_{50/50}$ and (b) $C_{75/25}$ cylinders.

Ag appears white, Cu grey and pores black on the images.

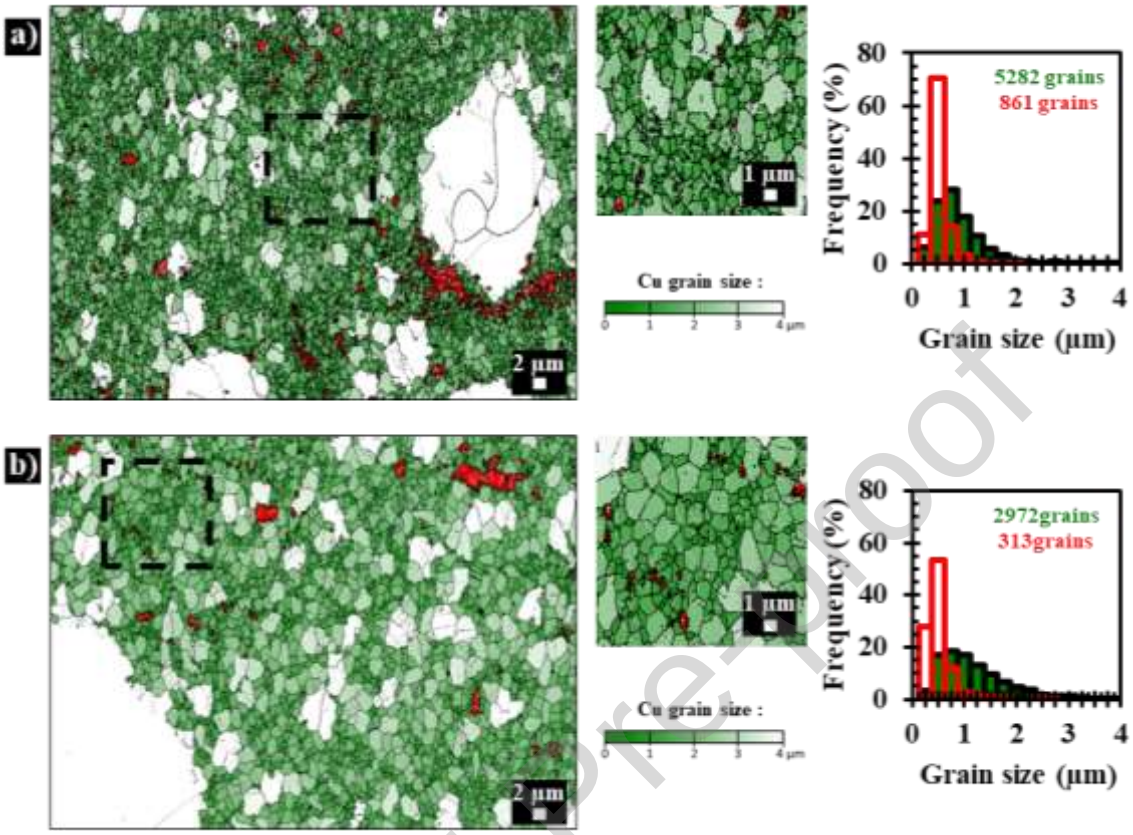

Fig. 4. Grain size distribution maps obtained by EBSD of the transverse section and the corresponding Cu and Ag grain size distributions for the $C_{50/50}$ (a) and $C_{75/25}$ (b) cylinders. Color code on the images, Ag : red, Cu : shades of green depending on the grain size calculated from equivalent circle diameter measurements (grains colored in white are larger than 4 µm), grain boundaries : black, ∑3 twin boundaries : grey and pores : black areas.

Cross sections of $C_{50/50}$ (Fig. 4a) and $C_{75/25}$ (Fig. 4b) were analysed by EBSD to determine the Cu and Ag grain size distributions. For the EBSD analysis, the size of the recorded maps is about 80 x 60 µm² while the largest grains from $Cu_{20µm}$ can reach 50 µm. The grain size distribution maps of the transverse section of $C_{50/50}$ (Fig. 4a) and $C_{75/25}$ (Fig. 4b) clearly reveal the bimodal size of the Cu grains. For practical reasons, the observed area is not large enough to provide relevant information on the Cu large grains fraction. The size distribution (obtained from EBSD analyses) of the smaller Cu grains is d_{10}=0.33 µm, d_{50}=0.68 µm, d_{90}=1.44 µm (5282 grains) for $C_{50/50}$ and d_{10} = 0.35 µm, d_{50} = 0.90 µm,

d_{90} = 2.04 µm (2972 grains) for $C_{75/25}$. This is similar to the $Cu_{1µm}$ powder (*cf* 2.1) and reflects the absence of grain growth during sintering at 450 °C with a short dwell time of 5 min. Moreover, the Cu grain size distribution is equivalent to that observed in C_{100} (d_{10} = 0.35 µm, d_{50} = 0.91 µm, d_{90} = 1.88 µm), an earlier sample prepared with $Cu_{1µm}$ only and sintered at 400 °C (5 min, 25 MPa) [15]. Nanoscale Ag is dispersed in the Cu fine-grains areas. Micrometric grains of Ag are localized in very large Ag agglomerates. For the Ag grains, d_{50} is equal to 0.35 and 0.31 µm for $C_{50/50}$ and $C_{75/25}$, respectively. This is higher than the value (0.17 µm) found for C_{100} [15]. By SPS sintering (427 °C, 5 min, 30 MPa) of a nanometric pure Ag powder, an increase in grain size from 86 to 500 nm has already been demonstrated [21]. Thus, the presence of large Cu grains which favour the agglomeration of Ag and the sintering temperature of 450 °C make possible the growth of Ag grains present in micrometer-sized agglomerates. The EBSD inverse pole figure maps according to the uniaxial pressing direction (WD) for $C_{50/50}$ and $C_{75/25}$ show no evidence of texturing after SPS sintering (Fig. 5), in line with previous studies [12] [14]. Crystallographic orientations moreover indicate that the "so-called" large Cu grains (originating from the $Cu_{20µm}$ powder) are polycrystalline aggregates.

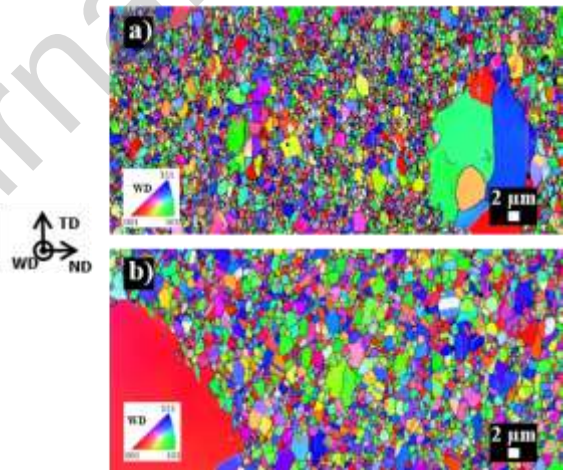

Fig. 5. EBSD inverse pole figure maps along the uniaxial pressing direction (WD) for the $C_{50/50}$ (a) and $C_{75/25}$ (b) cylinders.

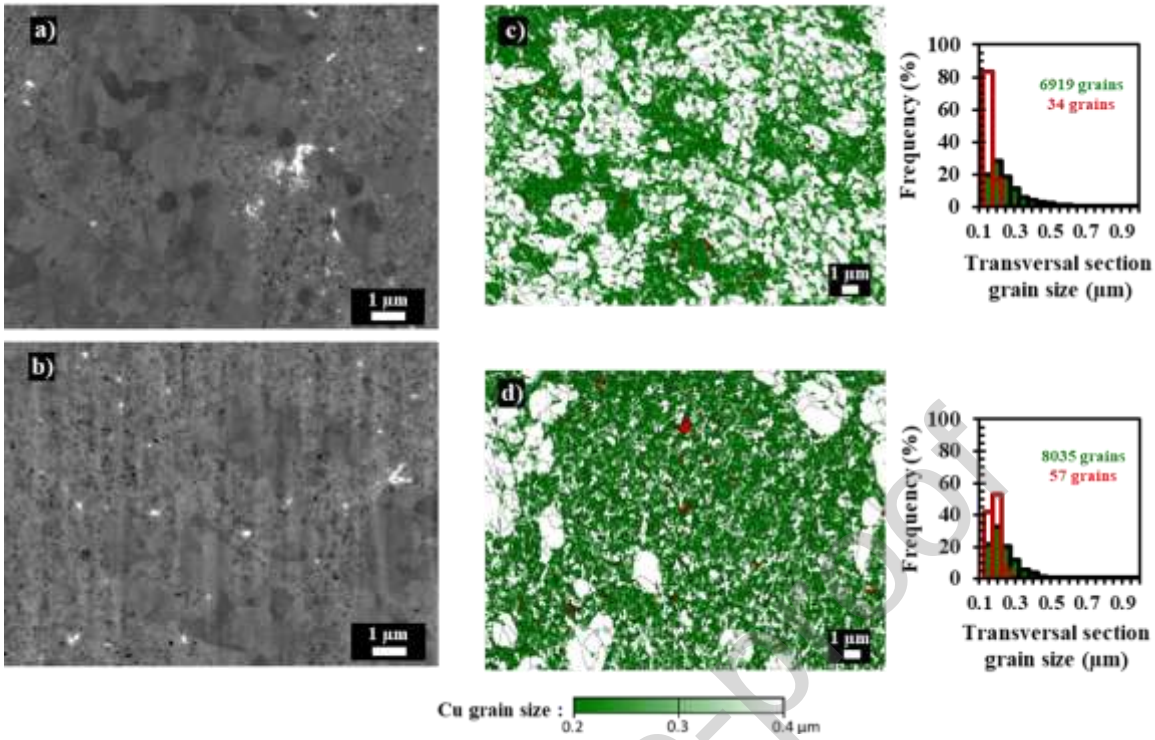

Fig. 6. Backscattered electrons SEM images (BSE) of the transversal section the $W_{50/50}$ (a) and $W_{75/25}$ (b) wires (Ø = 0.5 mm). Grain size distribution of the transversal section and the corresponding Cu and Ag grain size distribution for the $W_{50/50}$ (c) and $W_{75/25}$ (d) wires (Ø = 0.5 mm). Color code on the images. Ag: red. Cu: shades of green depending on the grain size calculated from equivalent circle diameter measurements (grains colored in white are larger than 0.4 µm). grain boundaries: black. ∑3 twin boundaries: grey and pores: black areas.

Increasingly finer wires are prepared by wire-drawing the cylinders at room temperature. The 4 mm in diameter wires are 98 % dense. For finer wires, the density is probably higher but the uncertainty is too high to give meaningful figures. SEM images of transverse sections of the $W_{50/50}$ and $W_{75/25}$ (Fig. 6) reveal the presence of a slight nanometric porosity (appearing black on the images) and the bimodal size of the Cu grains. Nanoscale Ag (appearing white on the images) is observed. The microstructure of $W_{50/50}$ and $W_{75/25,}$ 0.5 mm in diameter, was investigated by EBSD (Fig. 6 and Fig. 7) to determine the Cu and Ag grain size distributions. Assuming a homothetic wire-drawing deformation of the wires and the Cu grains, for a wire with a diameter of 0.5 mm, a Cu grain width of 0.4 µm is the result of the deformation of a Cu grain with an initial diameter approximately 6 µm. This value (6 µm) was chosen because Cu grains of this size are among the largest observed for $Cu_{1µm}$ and among the smallest observed

for $Cu_{20\mu m}$. Subsequently, grains resulting from the deformation of a $Cu_{1\mu m}$ powder will be called ex-$Cu_{1\mu m}$. They will be called ex-$Cu_{20\mu m}$ if they come from the deformation of a $Cu_{20\mu m}$ powder. The bimodal size of the Cu grains is observed for $W_{50/50}$ (Fig. 6c) and $W_{75/25}$ (Fig. 6d). The diameter of the ex-$Cu_{20\mu m}$ grains is in the range 0.4-2 µm. This large Cu grains are observed in higher proportion in $W_{50/50}$ (Fig. 6c) than in $W_{75/25}$ (Fig. 6d). The diameter of the fine Cu grains is in the range 0.1-0.4 µm. The Cu grain size distribution is d_{10} = 0.14 µm, d_{50} = 0.20 µm, d_{90} = 0.40 µm for $W_{50/50}$ and d_{10} = 0.14 µm, d_{50} = 0.20 µm, d_{90} = 0.33 µm for $W_{75/25}$. Both are close to that for W_{100} (d_{10} = 0.14 µm, d_{50} = 0.20 µm, d_{90} = 0.32 µm) [15]. Nanoscale Ag is dispersed in fine Cu fine-grains areas. Some large agglomerates (about 1 µm) are occasionally observed in agreement with the observations made on the cylinders. For both wires, the Ag grain size is about 0.16 µm, highlighting the grain refinement by wire-drawing. The Cu and Ag grain refinement in the transverse direction is accompanied by grains elongation in the drawing direction. Under the effect of successive drawing passes, Cu and Ag grains composing $W_{50/50}$ (Fig. 7a) and $W_{75/25}$ (Fig. 7b) are strongly elongated along the drawing axis as shown by their size distribution maps. The most part of ex-$Cu_{20\mu m}$ grains are several tens of micrometers long (indicated by an arrow in Fig. 7a and 7b). The fine nanometric grains of Cu and Ag are elongated by a few micrometers. From the transverse and longitudinal observations of the wires it is possible to consider that the large grains (ex-$Cu_{20\mu m}$) can be fast channels for electron transport because they form large and long areas with few grain boundaries and without Ag.

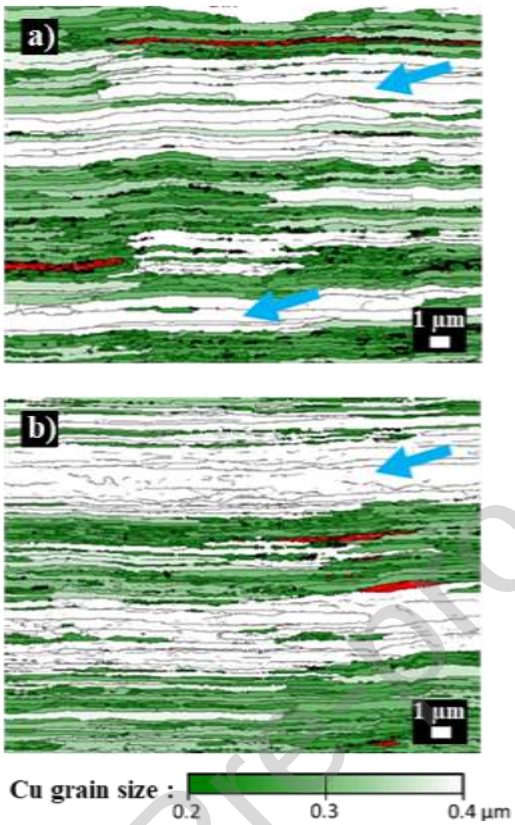

Fig. 7. Grain size distribution maps obtained by EBSD of the longitudinal section the $W_{50/50}$ (a) and $W_{75/25}$ (b) wires (Ø = 0.5 mm). Color code on the images. Ag: red. Cu: shades of green depending on the grain size (grains colored in white are larger than 0.4 µm). grain boundaries: black. ∑3 twin boundaries: grey and pores: black areas.

The EBSD inverse pole figure maps of cross-section of $W_{50/50}$ and $W_{75/25}$ in the direction of wire drawing (WD) are presented in Figure 8. For $W_{50/50}$ (Fig 8a), the grains are mostly oriented along <111> and <100> directions in the wire-drawing axis, which corresponds to the drawing texture of face-centred-cubic metals but it is important to note that some grains with a diameter higher than 0.4 µm (Fig 8b) present different orientations, which may reflect that the texturing of these grains is still ongoing. For $W_{50/50}$ the <100> and <111> orientations represent 49 % and 9 % of the image surface area, respectively. By contrast, $W_{75/25}$ is almost exclusively made up of grains oriented <111> and <100> (78 % and 12 % of the image surface area, respectively) (Fig. 8c) as could also be observed for W_{100} [15].

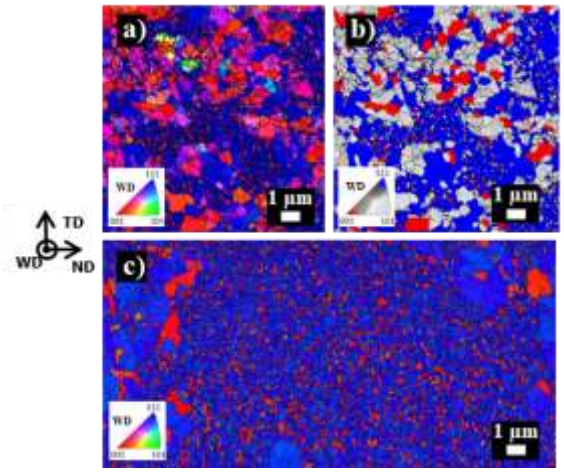

Fig. 8. EBSD inverse pole figure maps along the drawing direction for the $W_{50/50}$ wire (Ø = 0.5 mm) (a), same image showing only grains oriented along <111> and <001> directions with an angle tolerance of 10° (Other orientations are presented in grey) (b). EBSD inverse pole figure maps along the drawing direction for the $W_{75/25}$ wire (Ø = 0.5 mm) (c).

3.1 Mechanical properties and electrical resistivity

The Vickers microhardness was measured along the diameter of a cross-section of $C_{50/50}$ (Fig. 9). The values are close to either 75 $HV_{0.2}$ or 110 $HV_{0.2,}$ which could reflect measurements performed in areas made up of grains originating from the $Cu_{20µm}$ powder or from the $Cu_{1µm}$ powder, respectively. Indeed, the Vickers microhardness of C_{100} is about 119 $HV_{0.2}$ (Fig. 9) [15] and about 45-50 HV for pure annealed Cu with a grain size between 10 and 20 µm.

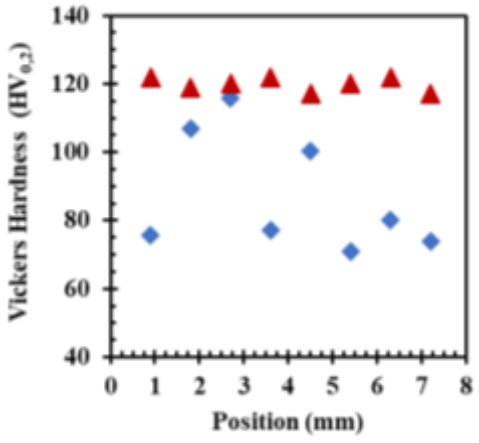

Fig. 9. Vickers microhardness along the diameter of a cross-section of the present $C_{50/50}$ (◆) and C_{100} (▲) [15].

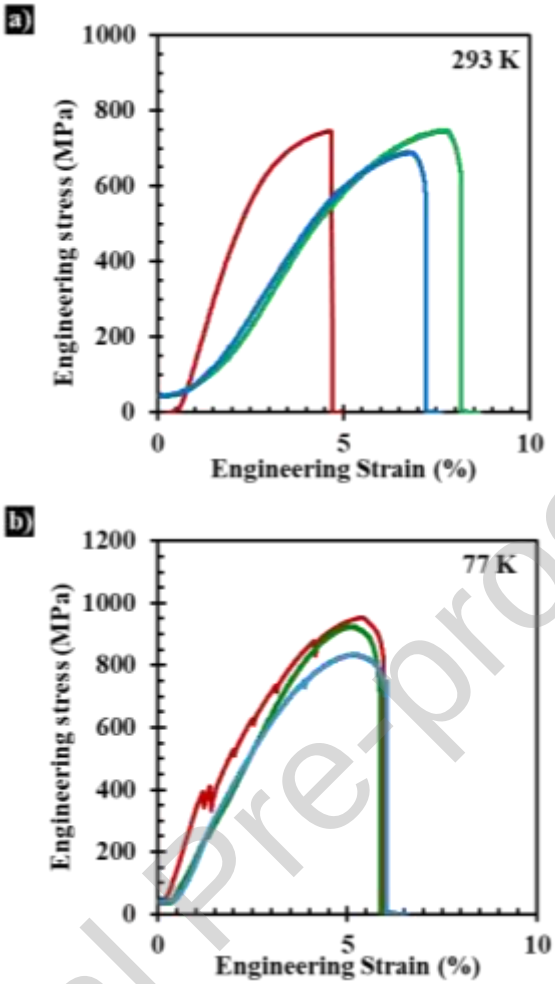

Fig. 10. Stress-strain curves at 293 K (a) and 77 K (b) for the 0.5 mm diameter wires: $W_{50/50}$ (—), $W_{75/25}$ (—) and W_{100} (—) [15].

Typical stress-strain curves for the 0.5 mm wires at 293 K and 77 K are shown in Figures 10a and 10b, respectively. During the tensile test, it was not possible to follow the strain with an extensometer due to the small diameter of wires and the testing itself being performed at 77 K. Strain was determined from crosshead displacement without any correction of the machine rigidity. Therefore, it is not possible to discuss strain values and only UTS values can be studied. The ultimate tensile strength of wires of decreasing diameter (1-0.2 mm) was measured at 293 K (Fig. 11a and Tab. 1) and at 77 K (Fig. 11b and Tab. 1). For the $W_{50/50}$ wires, the UTS value is in the range 586-791 MPa at 293 K and in the range 727-954 MPa at 77 K. For the $W_{75/25}$ wires, the values are higher (632-879 MPa at 293 K and 786-1082 MPa at 77 K). The higher values at 77 K could reflect the lower mobility of the dislocations at the liquid N_2

temperature. The UTS increase upon the decrease in wire diameter, reflecting the refinement of the microstructure. It is interesting to note that the present UTS are lower than those for W_{100} (689-914 MPa at 293 K and 805-1138 MPa at 77 K) [15], which contains only ex-$Cu_{1\mu m}$ grains. The decrease in the density of grain boundaries due to the presence of the large grains ex-$Cu_{20\mu m}$ decreases the density of obstacles opposing the movement of dislocations and could explain the progressively lower UTS for $W_{75/25}$ and $W_{50/50}$. UTS values of composite wires are higher than that obtained by the pure copper wires, thus reflecting the effect of mechanical reinforcement of the Ag as a discrete, nanometric, second phase. The Ag/Cu interfaces act as a brake on the movement of dislocations allowing an increase in mechanical strength of composite wires.

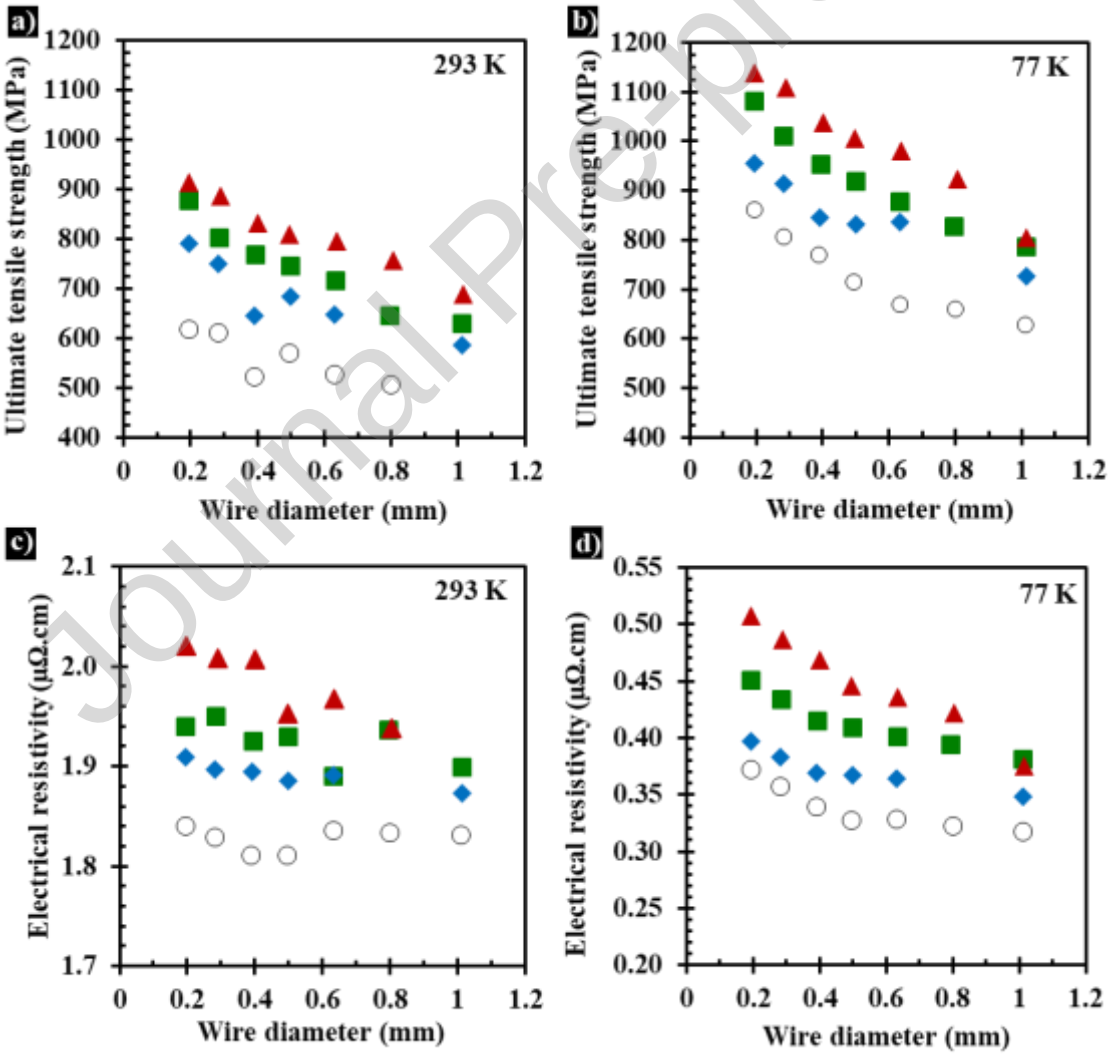

Fig. 11. UTS *vs* wire diameter at 293 K (a) and 77 K (b) and electrical resistivity *vs* wire diameter at 293 K (c) and 77 K (d) the present $W_{50/50}$ (◆) and $W_{75/50}$ (■) and SPS Cu (○) and W_{100} (▲) [15] wires.

Tab. 1. Electrical resistivity and ultimate tensile strength at 293 K and 77 K for different wires.

Sample	Wire diameter (mm)	Electrical resistivity at 293 K (μΩ.cm)	Electrical resistivity at 77 K (μΩ.cm)	Ultimate tensile strength at 293 K (MPa)	Ultimate tensile strength at 77 K (MPa)
$W_{50/50}$	1.0	1.87	0.35	586	727
	0.6	1.89	0.36	648	837
	0.5	1.89	0.37	686	831
	0.4	1.90	0.37	645	846
	0.3	1.90	0.38	750	915
	0.2	1.91	0.40	791	954
$W_{75/25}$	1.0	1.90	0.38	632	786
	0.8	1.94	0.39	647	828
	0.6	1.89	0.40	718	878
	0.5	1.93	0.41	746	919
	0.4	1.93	0.42	771	955
	0.3	1.95	0.43	803	1011
	0.2	1.94	0.45	879	1082
W_{100} [15]	1.0	1.78	0.38	689	805
	0.8	1.94	0.42	756	924
	0.6	1.97	0.44	795	981
	0.5	1.95	0.45	809	1006
	0.4	2.01	0.47	833	1038
	0.3	2.01	0.49	887	1109
	0.2	2.02	0.51	914	1138
Cu [15]	1.0	1.83	0.32	-	628
	0.8	1.83	0.32	508	660
	0.6	1.84	0.33	527	670
	0.5	1.81	0.33	571	714
	0.4	1.81	0.34	523	770
	0.3	1.83	0.36	611	807
	0.2	1.84	0.37	619	860

The electrical resistivity (Fig. 11 – Tab. 1) is in the range 1.87-1.91 μΩ.cm at 293 K and in the range 0.35-0.40 μΩ.cm at 77 K for $W_{50/50}$ and from 1.90 to 1.94 μΩ.cm at 293 K and from 0.38 to 0.45 μΩ.cm at 77 K for $W_{75/25}$ wires. The higher electrical resistivity of the finer wires is due to the increased density of grain boundaries, which act as scattering centers for conduction electrons. The lower values at 77 K can be explained by the negligible electron-phonon interactions at low temperature. The electrical resistivity of W_{100} is between 1.94 and 2.02 μΩ.cm at 293 K and between 0.38 and 0.51 μΩ.cm at 77 K. These results show that the addition of larger grains effectively decreases the density of

grain boundaries and allows a reduction in the electrical resistivity of the wires. Moreover, this decrease in resistivity is easily controlled by adjusting the proportion of larger grains in the starting powder. The electrical resistivity of composite wires is higher than that of pure copper wires [15]. This increase in electrical resistivity is a consequence of the presence of Ag/Cu interfaces which are diffusion centers for the conduction electrons.

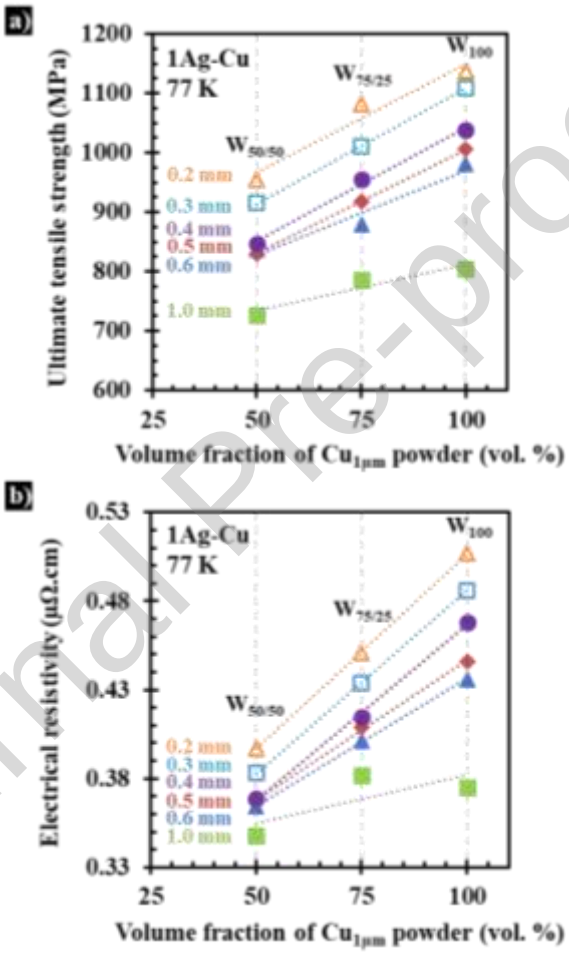

Fig. 12. (a) UTS (77K) for 1Ag-Cu wires of different diameters *vs* the proportion of $Cu_{1\mu m}$ and (b) electrical resistivity (77K) for wires of different diameters *vs* the proportion of $Cu_{1\mu m}$.

In order to study the effect of the grain-size distribution of the Cu matrix on the properties of the wires, the UTS and the electrical resistivity were plotted *vs* the initial $Cu_{1\mu m}$ proportion (Fig. 12) for all the wires studied. The proportion of fine Cu grains has a moderate effect on the UTS. From 1 mm to 0.2 the increase of the UTS value is about 31 % for $W_{50/50}$, it is about 37 % for $W_{75/25}$ and 42 % for

W_{100}. The slope of the different dote lines are not significantly different. For a given diameter, the change in the UTS value of a sample is simply due to the change in the number of grain boundaries, i.e. a change in the amount of obstacles blocking the movement of dislocations. Reducing the proportion of fine grains has a more pronounced effect on the electrical resistivity than on the UTS. Moreover, the slopes are increasingly steeper when the diameter decrease from 1.0 to 0.4 mm. This shows that the addition of large grains has a more significant effect on the electrical properties of the wires with smaller diameters (down to 0.4 mm). Then the slopes of the straight lines of 0.2, 0.3 and 0.4 mm wires are equal. This observation can be explained by the fact that an effect of size appears as soon as the dimensions of surface, interface or grains approach the electronic mean free path [22-24]. If the grain size is larger than the electron means free path, the electrical resistivity is expected to approach that of bulk Cu but if the dimensions of grains is smaller than the electron mean free path, grain boundary scattering dominates and hence contributing to the increase of the electrical resistivity. Effect of dimensions becomes non-negligible when the distance between surfaces or interfaces is less than 3 times the electronic mean free path. At 77 K, for annealed copper, the electron mean free path is about 330 nm. This means that grains smaller than 1 µm overly contribute to the increase in the electrical resistivity of the wires. In the case of $W_{50/50,}$ we observe a very weak increase in resistivity between the diameter of 1 mm and 0.4 mm, reflecting the presence of large micrometer-sized grains that serve as large channels for rapid electronic conduction and help maintain low electrical resistivity. However, for the most important wire-drawing deformations, the size of the large grains reaches a size less than three times the mean free path, explaining the faster increase in the electrical resistivity for the diameters 0.3 and 0.2 mm. $W_{75/25}$ presents the same evolution of the resistivity but in a less marked way in agreement with the higher initial proportion of $Cu_{1µm}$. For the W_{100} wires which are almost exclusively composed of ultra-thin grains, all the Cu grains contribute to the increase in electrical resistivity by size effect which has the effect that the electrical resistivity increases continuously when the diameter of W_{100} wires decreases. From 1 mm to 0.2 mm the increase in electrical resistivity value is about 14 % for $W_{50/50}$, it is about 18 % for $W_{75/25}$ and 38 % for W_{100}.

The UTS *vs.* electrical resistivity plot at 77 K for 1Ag-Cu wires is shown in Figure 13. The slope for $W_{50/50}$ and $W_{75/25}$ is steeper compared to that for W_{100} according to Figure 12. For the 0.2 mm wires, $W_{50/50}$ presents the lowest electrical resistivity but also the lowest UTS (0.40 μΩ.cm; 954 MPa), W_{100} presents the highest UTS but also the highest electrical resistivity (0.51 μΩ.cm; 1138 MPa) and $W_{75/25}$ is a good compromise between high UTS and low resistivity (0.45 μΩ.cm; 1082 MPa). Thus, by adding large grains to the Cu matrix, the resistivity of the wires is greatly reduced. At equivalent UTS (about 1100 MPa) the electrical resistivity of $W_{75/25}$ is 12 % lower than that of W_{100}. Thanks to an additional step that is simple to implement (adding large grains of copper during the preparation of the composite powder) it is possible to significantly improve the compromise between high UTS and low electrical resistivity. However, the proportion between fine and large Cu grains must be chosen carefully because although very effective in reducing electrical resistivity, the large grains content should not be too high at the risk of making the wire mechanically too weak.

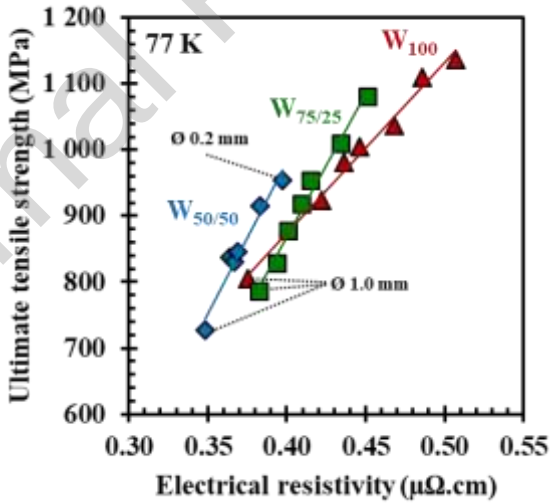

Fig. 13. UTS vs electrical resistivity at 77 K for wires with diameter from 1 mm to 0.2 mm for $W_{50/50}$ (◆), $W_{75/50}$ (■) and W_{100} (▲) [15]. The dotted lines are used to indicate wires with a diameter of 1 mm and the 0.2 mm wire in the case of $W_{50/50}$.

4 CONCLUSIONS

By a method combining powder metallurgy, SPS sintering and wire drawing, it is possible to prepare 1 vol. % Ag-Cu composite wires with a Cu matrix showing a bimodal grain-size distribution. It has been shown that the bimodal character of Cu is preserved after all the preparation steps, namely after the preparation of the powder, the SPS cylinders and the wires. The present wires are composed of Ag nanowires distributed at the boundaries of fine Cu grains whose size is close to that of a dislocation cell (0.2 µm) and large and long micrometric Cu grains. Because they form large areas with few grain boundaries micrometric Cu grains can be considered as fast channels for electron transport. Thus, at 77 K, the electrical resistivity of 0.2 mm wires is 0.51 µΩ.cm for W_{100}, 0.45 µΩ.cm for $W_{75/25}$, 0.40 µΩ.cm for $W_{50/50}$. Interestingly, the presence of the larger Cu grains allows to greatly reduce the electrical resistivity while having a more moderate effect on the UTS values of the wires. At 77 K, UTS value is 1138 MPa for W_{100}, 1082 MPa for $W_{75/25}$ and 954 MPa for $W_{50/50}$. The $W_{75/25}$ wires offer the best combination of high tensile strength low electrical resistivity. It is thus demonstrated that it is possible to improve the low resistivity and high mechanical strength compromise by a simple modification of the initial composite powder. In addition, it is possible to adapt, if necessary, the properties of prepared wires by modifying the initial proportion of fine and coarse Cu grains. These results could provide important guidelines for the design and preparation of ultra-strong yet electrically conducting macroscopic wires.

DECLARATION OF INTEREST

The authors declare that they have no known financial interests or personal relationships that could have appeared to influence the work reported in this paper.

ACKNOWLEDGEMENTS

This work was financially supported by the Agence Nationale de la Recherche (ANR-20-CEO8-0027). The authors thank Dr. C. Josse (Centre de microcaractérisation Castaing), Dr. A. Weibel (CIRIMAT),

Y. Borjon-Piron (CIRIMAT), Dr. G. Rikken (LNCMI) and Dr. C. Verdy (LERMPS, Sevenans, France) for discussions. Dr. C. Verdy is also thanked for providing a Cu powder sample.

DATA AVAILABILITY

Data will be made available on request.

REFERENCES

[1] S. Askénazy, Analytical solution for pulsed field coils placed in a magnetic field, Phys. B, 211 (1995), pp. 56-64. https://doi.org/10.1016/0921-4526(94)00944-Q.

[2] Y. Sakai, K. Inoue, T. Asano, H. Wada, and H. Maeda, Development of high-strength, high-conductivity Cu-Ag alloys for high-field pulsed magnet use, Appl. Phys. Lett., 9 (1991), pp. 2965-2967. https://doi.org/10.1063/1.105813.

[3] K. Han, A. Baca, H. Coe, J. Embury, K. Kihara, B. Lesch, L. Li, J. Schillig, J. Sims, S. Van Sciver and H.J. Schneider-Muntau, Material issues in the 100 T non-destructive magnet, IEEE Trans. Appl. Supercond., 10 (2000), pp. 1277-1280. https://doi.org/10.1109/77.828468.

[4] K. Han, J.D. Embury, J.R. Sims, L.J. Campbell, H.J. Schneider-Muntau, V.I. Pantsyrnyi, A. Shikov, A. Nikulin and A. Vorobieva, The fabrication, properties and microstructure of Cu–Ag and Cu–Nb composite conductors, Mater. Sci. Eng. A, 267 (1999), pp. 99-114. https://doi.org/10.1016/S0921-5093(99)00025-8.

[5] X. Zuo, K. Han, C. Zhao, R. Niu and E. Wang, Microstructure and properties of nanostructured Cu 28 wt%Ag microcomposite deformed after solidifying under a high magnetic field, Mater. Sci. Eng. A, 619 (2014), pp. 319-327. https://doi.org/10.1016/j.msea.2014.09.070.

[6] F. Dupouy, S. Askenazy, J. P. Peyrade, D. Legat, Composite conductors for high pulsed magnetic fields, Phys. B, 211 (1995), pp. 43-45. https://doi.org/10.1016/0921-4526(94)00934-N.

[7] J. Béard, J. Billette, N. Ferreira, P. Frings, J-M. Lagarrigue, F. Lecouturier and J-P. Nicolin, Design and tests of the 100 Tesla triple coil at LNCM, IEEE Trans. Appl. Supercond., 28 (2018), Article 4300305. https://doi.org/10.1109/TASC.2017.2779817.

[8] K. Spencer, F. Lecouturier, L. Thilly, and J. D. Embury, Established and emerging materials for use as high-field magnet conductors, Adv. Eng. Mater., 6 (5) (2004), pp. 290-297. https://doi.org/10.1002/adem.200400014.

[9] N. Nguyen, J. Michel and C. H. Mielke, Status and Development of Pulsed Magnets at the NHMFL Pulsed Field Facility, IEEE Trans. Appl. Supercond., 26 (4) (2016), Article 4300905. https://doi.org/10.1109/TASC.2016.2515982.

[10] V. Pantsyrny, A. Shikov, A. Vorobieva, N. Khlebova, N. Kozlenkova, I. Potapenko, M. Polikarpova, Stability aspects of the high strength high conductivity microcomposite Cu-Nb wires properties, IEEE Trans. Appl. Supercond., 16 (2) (2006), pp. 1656-1659. https://doi.org/10.1109/TASC.2006.870554.

[11] D. Raabe, P.-P. Choi, Y. Li, A. Kostka, X. Sauvage, F. Lecouturier, K. Hono, R. Kirchheim, R. Pippan, D. Embury, Metallic composites processed via extreme deformation: Toward the limits of

strength in bulk materials, MRS Bull., 35 (12) (2010), pp. 982-991. https://doi.org/10.1557/mrs2010.703.

[12] C. Arnaud, F. Lecouturier, D. Mesguich, N. Ferreira, G. Chevallier, C. Estournès, A. Weibel and C. Laurent, High strength – high conductivity double-walled carbon nanotube - Cu composite wires, Carbon, 96 (2016), pp. 212-215. https://doi.org/10.1016/j.carbon.2015.09.061.

[13] D. Mesguich, C. Arnaud, F. Lecouturier, N. Ferreira, G. Chevallier, C. Estournès, A. Weibel, C. Josse and C. Laurent, High strength-high conductivity carbon nanotube-Cu wires with bimodal grain size distribution by spark plasma sintering and wire-drawing, Scripta Mater., 137 (2017), pp. 78-82. https://doi.org/10.1016/j.scriptamat.2017.05.008.

[14] S. Tardieu, D. Mesguich, A. Lonjon, F. Lecouturier, N. Ferreira, G. Chevallier, A. Proietti, C. Estournès and C. Laurent, Nanostructured 1% Ag-Cu composite wires with a high tensile strength and a high electrical conductivity, Mater. Sci. Eng. A, 761 (2019), Article 138048. https://doi.org/10.1016/j.msea.2019.138048.

[15] S. Tardieu, D. Mesguich, A. Lonjon, F. Lecouturier, N. Ferreira, G. Chevallier, A. Proietti, C. Estournès and C. Laurent, Influence of alloying on the tensile strength and electrical resistivity of Ag nanowire - Cu composites macroscopic wires, J. Mater. Sci., 56 (2021), pp. 4884-4895. https://doi.org/10.1007/s10853-020-05556-9.

[16] Y. Wang, M. Chen, F. Zhou, E. Ma, High tensile ductility in a nanostructured metal, Nature, 419 (2002), pp. 912-915. https://doi.org/10.1038/nature01133.

[17] Z. Lai, Y. Mai, H. Song, J. Mai, X. Jie, Heterogeneous microstructure enables a synergy of strength, ductility and electrical conductivity in Cu alloys, J. Alloys Compd., 902 (2022), Article 163646. https://doi.org/10.1016/j.jallcom.2022.163646.

[18] X. Hou, S. Krauß, B. Merle, Additional grain boundary strengthening in length-scale architectured Cu with ultrafine and coarse domains, Scr. Mater., 165 (2019), pp. 55-59. https://doi.org/10.1016/j.scriptamat.2019.02.019.

[19] P. Coddet, C. Verdy, C. Coddet, F. Debray, Effect of cold work, second phase precipitation and heat treatments on the mechanical properties of copper–silver alloys manufactured by cold spray, Mater. Sci. Eng. A, 637 (2015), pp. 40-47. https://doi.org/10.1016/j.msea.2015.04.008.

[20] A. Lonjon, I. Caffrey, D. Carponcin, E. Dantras, C. Lacabanne, High electrically conductive composites of Polyamide 11 filled with silver nanowires: nanocomposites processing, mechanical and electrical analysis, J. Non-Cryst. Solids, 376 (2013), pp. 199-204. https://doi.org/10.1016/j.jnoncrysol.2013.05.020.

[21] T. Mineta, T. Saito, T. Yoshihara, H. Sato, Structure and mechanical properties of nanocrystalline silver prepared by spark plasma sintering, Mater. Sci. Eng. A, 754 (2019), pp. 258-264. https://doi.org/10.1016/j.msea.2019.03.101.

[22] R. B. Dingle, The electrical conductivity of thin wires, Proc. R. Soc. Lond. A, 201 (1950), pp. 545-560. https://doi.org/10.1098/rspa.1950.0077.

[23] H. Gleiter, Nanocrystalline materials, Progress in Materials Science, 33 (4) (1989), pp. 223-315. https://doi.org/10.1016/0079-6425(89)90001-7.

[24] T. Gu, J.-R. Medy, F. Volpi, O. Castelnau, S. Forest, E. Hervé-Luanco, F. Lecouturier, H. Proudhon, P.-O. Renault, L. Thilly, Multiscale modeling of the anisotropic electrical conductivity of architectured and nanostructured Cu-Nb composite wires and experimental comparison, Acta Materialia, 141 (2017), pp. 131-141. https://doi.org/10.1016/j.actamat.2017.08.066.

Author contributions:

Simon Tardieu : Investigation, Formal analysis, Writing - Original draft preparation, Reviewing and Editing; **David Mesguich :** Resources, Investigation, Writing - Reviewing and Editing **; Antoine Lonjon :** Resources, Investigation, Writing - Reviewing and Editing ; **Florence Lecouturier-Dupouy:** Supervision, Writing - Original draft preparation, Reviewing and Editing ; **Nelson Ferreira:** Resources, Investigation; **Geoffroy Chevallier:** Resources, Investigation; **Claude Estournès:** Supervision, Writing - Reviewing and Editing ; **Arnaud Proietti** Investigation Writing- Reviewing and Editing **; Christophe Laurent:** Supervision, Writing- Original draft preparation, Reviewing and Editing.

DECLARATION OF INTEREST

The authors declare that they have no known financial interests or personal relationships that could have appeared to influence the work reported in this paper.

Graphical abstract

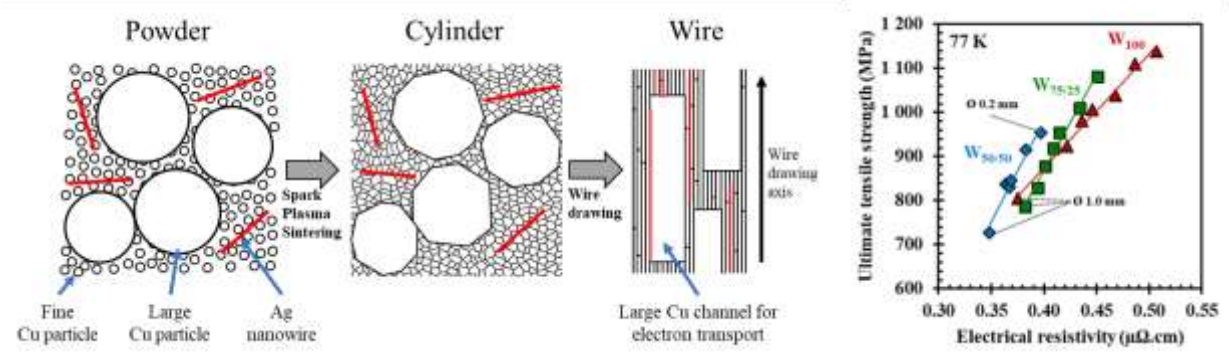

HIGHLIGHTS

- The larger copper grains act as channels for fast electron conduction thus allowing to maintain a low electrical resistivity (0.45 μΩ.cm, at 77 K).
- Compared to wires with only fine-grained copper, this represents a 12 % lower electrical resistivity for an equivalent ultimate tensile strength (1082 MPa at 77 K), which is provided by the finer copper grains and the silver nanowires.
- It is possible to improve the low resistivity - high ultimate tensile strength compromise of the composite wires by simply adding large grains of Cu during the composite powder preparation step.
- The strength-resistivity trade-off can be fine-tuned simply by adjusting the large grain / fine grain proportion.